RESEARCH ARTICLE | OCTOBER 10 2023

Magnetocrystalline anisotropy of interstitially and substitutionally Sn-doped MnBi for high temperature permanent magnet applications

Minyeong Choi ; Yang-Ki Hong ; Hoyun Won ; Chang-Dong Yeo ; Byung-Chul Choi ; Jihoon Park ; Woncheol Lee

AIP Advances 13, 105015 (2023)
https://doi.org/10.1063/5.0166930

Magnetocrystalline anisotropy of interstitially and substitutionally Sn-doped MnBi for high temperature permanent magnet applications

Cite as: AIP Advances 13, 105015 (2023); doi: 10.1063/5.0166930
Submitted: 8 July 2023 • Accepted: 7 September 2023 •
Published Online: 10 October 2023

Minyeong Choi,[1] Yang-Ki Hong,[1,a)] Hoyun Won,[1] Chang-Dong Yeo,[2,a)] Byung-Chul Choi,[3] Jihoon Park,[4] and Woncheol Lee[5]

AFFILIATIONS

[1] Department of Electrical and Computer Engineering, The University of Alabama, Tuscaloosa, Alabama 35487, USA
[2] Department of Mechanical Engineering, Texas Tech University, Lubbock, Texas 79409, USA
[3] Department of Physics and Astronomy, University of Victoria, Victoria, British Columbia V8P 5C2, Canada
[4] Korea Institute of Materials Science, Changwon, South Korea
[5] Samsung Electronics, Co. Ltd., Suwon, South Korea

[a)] **Authors to whom correspondence should be addressed:** ykhong@eng.ua.edu and changdong.yeo@ttu.edu

ABSTRACT

First-principles calculations were performed to calculate the electronic structures of low temperature phase (LTP) MnBi ($Mn_{50}Bi_{50}$) and substitutionally and interstitially Sn-doped MnBi [$Mn_{50}Bi_{25}Sn_{25}$, $(Mn_{0.5}Bi_{0.5})_{66.7}Sn_{33.3}$]. Brillouin function predicts the temperature dependence of saturation magnetization M(T). Sn substitution for Bi in MnBi ($Mn_{50}Bi_{25}Sn_{25}$) changes the magnetocrystalline anisotropy constant (K_u) from −0.202 MJ/m^3 (the in-plane magnetization) for LTP MnBi to 1.711 MJ/m^3 (the out-of-plane magnetization). In comparison, the K_u remains negative but slightly decreases to −0.043 MJ/m^3 when Sn is interstitially doped in MnBi [$(Mn_{0.5}Bi_{0.5})_{66.7}Sn_{33.3}$]. The Curie temperature (T_C) decreases from 716 K for LTP $Mn_{50}Bi_{50}$ to 445 K for $Mn_{50}Bi_{25}Sn_{25}$ and 285 K for $(Mn_{0.5}Bi_{0.5})_{66.7}Sn_{33.3}$. $Mn_{50}Bi_{25}Sn_{25}$ has a lower magnetic moment of 5.034 μ_B/f.u. but a higher saturation magnetization of 64.2 emu/g than $(Mn_{0.5}Bi_{0.5})_{66.7}Sn_{33.3}$ with a magnetic moment of 6.609 μ_B/f.u. and a saturation magnetization of 48.2 emu/g because the weight and volume of the substitutionally Sn-doped MnBi are smaller than the interstitially Sn-doped MnBi. The low Curie temperature and magnetization for Sn-doped MnBi are attributed to the high concentration of Sn. Thus, future study needs to focus on low Sn-concentrated MnBi.

I. INTRODUCTION

Nd–Fe–B alloy is a rare-earth permanent magnet with the highest maximum energy product $(BH)_{max}$ at 300 K among currently available permanent magnets. Its Curie temperature (T_C) is 523 K, which is close to the 473 K of the motor operating temperature for electric vehicles. The $(BH)_{max}$ of Nd–Fe–B significantly decreases as temperature increases due to its large negative temperature coefficient of the coercivity (H_{Ci}), namely α, and low T_C.[1,2] To improve the thermomagnetic stability of Nd–Fe–B, Dy partially substituted Nd, i.e., $Nd_{1-x}Dy_x$–Fe–B; therefore, the negative temperature coefficient decreased.[3] The rare-earth minerals supply chain recently became unstable, and rare-earth Nd and Dy elements are expensive. Thus, investigating rare-earth free permanent magnetic materials with a high $(BH)_{max}$, high T_C, and low cost is an emerging topic. For this reason, Mn-based alloys receive great attention because Mn has the highest magnetic moment among transition metals (TMs) and is inexpensive. However, the Mn element is antiferromagnetic but becomes ferromagnetic when Mn is alloyed with other elements, such as Bi or Al.

The NiAs-type hexagonal MnBi shows a positive temperature coefficient of coercivity up to about 550 K[4,5] and 700 K of T_C;[5] therefore, high-temperature applications of MnBi are foreseeable. Sakuma *et al.* reported 2 MJ/m^3 of the magnetocrystalline anisotropy

constant (K_u) at 300 K and −0.5 MJ/m^3 at 0 K,[6] much higher than −0.202 MJ/m^3 at 0 K.[7] The above K_u of MnBi implies that the magnetic spins are in the out-of-plan at 300 K and the in-plane at 0 K.

Magnetocrystalline anisotropy of MnBi can be tuned by either temperature or transition metal element(s) substitution for Mn or Bi. The spin configuration of the LTP-MnBi is changed from the in-plane (<84 K) to the out-of-plane (>84 K).[8] Hong *et al.* reported that the K_u of MnBi is changed from −0.35 MJ/m^3 for MnBi to 1.90 MJ/m^3 for interstitial doping of Co in MnBi and 1.62 MJ/m^3 for Co-Fe doping.[9] Partial substitution of Sn for Bi in $MnBi_{1-x}Sn_x$ changes K_u from −0.5 MJ/m^3 at x = 0.0 to about 3 MJ/m^3 at x = 0.1.[6] Interstitial doping of Co in MnBi increases K_u from 2.07 to 3.06 MJ/m^3.[10]

Interstitial doping of Cu in MnBi prevents Mn from diffusion into bipyramidal (interstitial) sites, weakening antiferromagnetic coupling between Mn at the main lattice and the interstitial Mn.[7] It is, therefore, of interest to tune the magnetocrystalline anisotropy of MnBi at the ground state by substitutional or interstitial metal element doping in MnBi and to investigate the temperature dependence of saturation magnetization and Curie temperature, and this is the aim of this work. Bismuth (Bi) is one of the critical minerals defined by the US government (the US Geological Survey) because it is mostly imported and prone to supply chain disruption.[11] Therefore, we chose the Sn element as a doping element in this work because of its melting temperature of 544 K, which is close to 505 K of Bi. The temperature dependence of magnetization of doped-MnBi was not yet reported.

In this work, we investigated the Sn doping effects on magnetic properties and T_C of MnBi [$Mn_{50}Bi_{25}Sn_{25}$, $(Mn_{0.5}Bi_{0.5})_{66.7}Sn_{33.3}$] using the first-principles calculations.

II. CALCULATION METHOD AND CRYSTAL STRUCTURE

A. Method of calculations

After having relaxed substitutionally or interstitially Sn-doped MnBi [$Mn_{50}Bi_{25}Sn_{25}$ or $(Mn_{0.5}Bi_{0.5})_{66.7}Sn_{33.3}$], the Kohn–Sham equation, $\hat{H}_{KS}\Psi(r) = \varepsilon_i\Psi(r)$, is solved with the relaxed lattice constants. The Hamiltonian ($\hat{H}_{KS}$) for the Kohn–Sham equation consists of the kinetic energy, nuclei energy (lattice potential), and a sum of the electron exchange and correlation energies (interaction),

$$\hat{H}_{KS} = \sum_i \left[-\frac{\hbar^2\Delta_i}{2m_e} + \sum_l \frac{-e^2}{4\pi\varepsilon_0}\frac{Z_l}{|r_i - R_l|} \right] + \frac{1}{2}\sum_{i\neq j}\frac{e^2}{4\pi\varepsilon_0}\frac{1}{|r_i - r_j|}. \quad (1)$$

The corresponding wave function is $\Psi(r) = \sum C_{kn}\varphi_{kn}$, where the wave ($\varphi_{kn}$) consists of a partial atomic wave in an atomic sphere (*as*) and a plane wave of the interstitial region (*ir*) of the MnBi unit cell. The total electron density is as follows:

$\rho_{as} = \sum_{E_k \le E_F} \Psi^*_{as}\Psi_{as}$ for $r <$ atomic radius,

$\rho_{ir} = \sum_{E_k \le E_F} \Psi^*_{ir}\Psi_{ir}$ for $r >$ atomic radius.

The partial atomic wave is $\phi_{k_n} = [A^K_{lm}u_l(r,\varepsilon) + B^K_{lm}\dot{u}_l(r,\varepsilon)]Y_{lm}(r)$, and the plane wave is $\phi_{k_n} = e^{i(k+Kn)r}$. A^K_{lm} and B^K_{lm} are the coefficients for matching the plane wave. u_l is the numerical solution of the radial Schrödinger equation in a given spherical potential. u_l is the energy derivative of u_l. Y_{lm} is the spherical harmonic of angular momentum l and quantum number m. After summing ρ_{as} and ρ_{ir}, we obtain the total electron density and construct the electron density map.

The WIEN2k package, based on density functional theory (DFT) within the local-spin-density approximation (LSDA) and using the full-potential linearized augmented plane wave (FPLAPW) method, is used to conduct the first-principles calculations.[12] All calculations use 19 × 19 × 27 k-point mesh, generating 1400 k-points in the irreducible part of the Brillouin zone.

Regarding magnetocrystalline anisotropy calculation, after adding spin–orbit coupling Hamiltonian (H_{SO}), $H_{SO} = -\frac{e\hbar}{4m^2c^2}\sigma \cdot \nabla\varphi(r) \times p = -\frac{e\hbar^2}{2m^2c^2}\frac{1}{r}\frac{d\varphi}{dr}L \cdot S$, where c is the speed of light, V is the potential energy of the electron, σ is the spin vector, L is the angular momentum vector, and S is the spin angular momentum vector, to the Hamiltonian (H_{KS}), the Kohn–Sham equation is solved for the magnetocrystalline anisotropy energy (ΔE_{MAE}),

$$\Delta E_{MAE} = \sum_i \varepsilon_i(\hat{n}_1) - \sum_i \varepsilon_i(\hat{n}_2) = E^{total}(\hat{n}_1) - E^{total}(\hat{n}_2), \quad (2)$$

where $\hat{n}_1$ and $\hat{n}_2$ are easy and hard spin directions, respectively. Magneto-crystalline anisotropy energy (MAE) was calculated using the total energy difference between ⟨100⟩ and ⟨001⟩ spin configurations ($\Delta E = E_{\langle 100\rangle} - E_{\langle 001\rangle}$).

To predict the temperature dependence of saturation magnetization, M_S(T), one needs the Curie temperature (T_C). The exchange integrals (J_{0j}) are calculated by the energy difference between the ground and excited states for the T_C calculation. The exchange integral can be expressed by $J_{ij} = (\Delta_{ij} - \Delta_i - \Delta_j)/(4S_iS_jn_iz_{ij})$, where S_i is the quantum spin of the ith Mn atom, Δ_i is the exchange energy difference between the ground and excited states when the ith Mn atom is reversed, n_i is the number of the ith atom, and z_{ij} is the number of neighboring the jth atom to the ith atom.[13] The exchange integrals (J_{0j}) consider interactions over all neighboring spins, then $J_0 = \sum_j J_{0j}$.[14] The T_C is then calculated with J_0 using the following mean-field approximation (MFA):[15]

$$T_c = \frac{2}{3k_B}J_0\gamma, \quad (3)$$

where J_0 is the molecular field parameter calculated by the summation of the exchange integrals J_{0j}, and k_B is the Boltzmann constant (1.38 × 10^{-23} J/K). The factor γ equals S(S + 1)/S^2, where S is the spin angular momentum.

Now, the temperature dependence of saturation magnetization M_S(T) is described by Eq. (4), i.e., the Brillouin function [$B(J, a')$]. Thus, one incorporates both $M_S(0)$ and T_C into Eq. (4) to calculate M_s(T),[16]

$$M_s(\mathrm{T}) = M_s(0)\left(\frac{2J+1}{2J}\coth\left(\frac{2J+1}{2J}a'\right) - \frac{1}{2J}\coth\left(\frac{a'}{2J}\right)\right) = M_s(0)B(J,a'), \quad (4)$$

where $a' = \frac{M/M_0}{T/T_c}\left(\frac{3}{J+1}\right)$, and J is the total angular momentum quantum number.

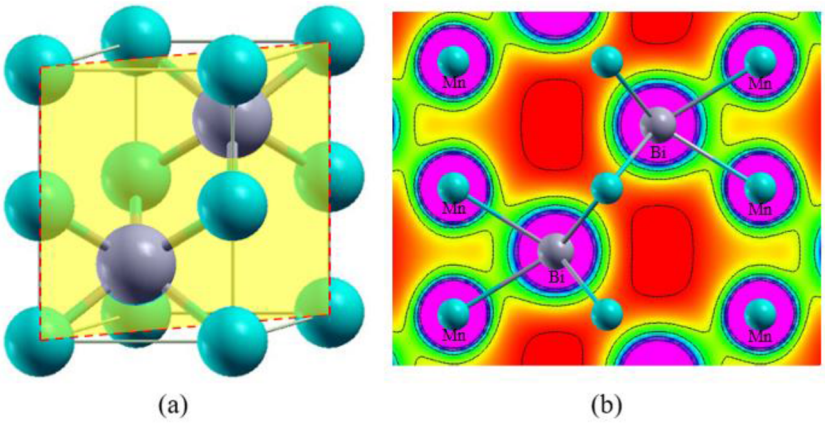

FIG. 1. (a) $(11\bar{2}0)$ plane and (b) electron density map for MnBi.

B. Electron density map

Figure 1 shows the $(11\bar{2}0)$ plane and the electron density map for the LTP-MnBi. The electron density map shows the valence electronic charge density differences in the plane containing Bi and vacant interstitial sites. The red color represents the least electron charge density. MnBi exhibits low electron charge density at two interstitial sites of the unit cell; therefore, large trigonal–bipyramidal interstitial sites are available for dopant or Mn atoms. Antropov *et al.* and Rania *et al.* studied the electron density map for doping the third element into the pyramidal sites,[10,17] which is a good agreement with the electron density map in this work. Therefore, there are two interstitial sites available for Sn doping.

1. Crystal structure

Figure 2 shows the crystal structures of MnBi and the substitutionally and interstitially Sn-doped MnBi. LTP-MnBi has two Mn atoms of (0, 0, 0) and (0, 0, 1/2) sites, and the Bi atoms of (1/3, 2/3, 1/4) and (2/3, 1/3, 3/4) sites. Sn substitutes for the Bi atom in the (2/3, 1/3, 3/4) site, namely substitutional Sn-doped MnBi ($Mn_{50}Bi_{25}Sn_{25}$). Otherwise, the two Sn atoms are inserted into the (2/3, 1/3, 1/4) and (1/3, 2/3, 3/4) sites, namely interstitial Sn-doped MnBi [$(Mn_{0.5}Bi_{0.5})_{66.7}Sn_{33.3}$]. Lattice parameters are determined after having the MnBi-Sn unit cell relaxed, and the parameters are listed in Table I. These parameters are used in first-principles calculation. The lattice parameters of LTP MnBi are

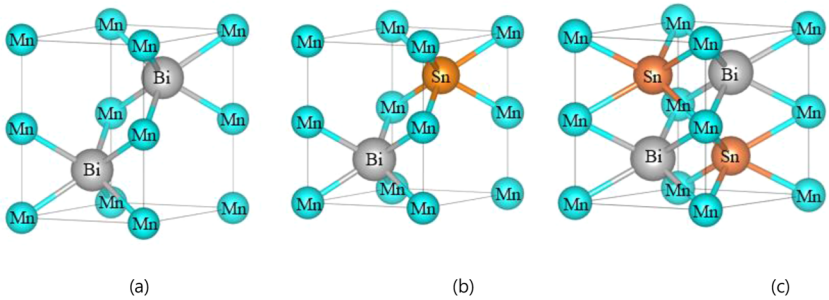

FIG. 2. Crystal structure (unit cell) of (a) LTP-MnBi ($Mn_{50}Bi_{50}$), (b) ($Mn_{50}Bi_{25}Sn_{25}$), and (c) $(Mn_{0.5}Bi_{0.5})_{66.7}Sn_{33.3}$.

TABLE I. Lattice constant of LTP-MnBi and substitutionally and interstitially Sn-doped MnBi.

		Lattice constant (Å)			
Materials	Type	$a = b$	c	Volume (Å^3)	c/a
$Mn_{50}Bi_{50}$	LTP	4.287	6.118	97.37	1.43
$Mn_{50}Bi_{25}Sn_{25}$	Substitutional	3.954	5.456	73.87	1.38
$(Mn_{0.5}Bi_{0.5})_{66.7}Sn_{33.3}$	Interstitial	4.611	5.683	104.63	1.23

a = 4.287 Å and c = 6.118 Å. The c/a ratio decreases by Sn doping in Table I, and the volume increases with interstitial Sn doping.

III. RESULTS AND DISCUSSION

We have calculated the total energy to determine spin configurations for LTP-MnBi and substitutionally or interstitially Sn-doped MnBi, showing the ferromagnetic spin configuration.

Figure 3 shows the DOS diagrams for LTP-MnBi, $Mn_{50}Bi_{25}Sn_{25}$, and $(Mn_{0.5}Bi_{0.5})_{66.7}Sn_{33.3}$. Spin-polarization is dominant in contributing to the DOS. Significant changes in the DOS are observed for $Mn_{50}Bi_{25}Sn_{25}$. The states of minority spin (down-spin) for $Mn_{50}Bi_{25}Sn_{25}$ below the Fermi energy (E_F) dramatically increase near −0.1 Ry compared to the DOS of LTP-MnBi in Fig. 2(a). In addition, the states of minority spin of $(Mn_{0.5}Bi_{0.5})_{66.7}Sn_{33.3}$ slightly increase compared to the DOS in Fig. 2(a). Thus, these decrease the magnetic moment per formula unit ($f.u.$) of $Mn_{50}Bi_{25}Sn_{25}$ and $(Mn_{0.5}Bi_{0.5})_{66.7}Sn_{33.3}$. Table II summarizes the calculated magnetic moments with corresponding saturation magnetization (M_S). Spin polarization dominantly contributes to the total magnetic moment of the LTP-MnBi and $Mn_{50}Bi_{25}Sn_{25}$ and $(Mn_{0.5}Bi_{0.5})_{66.7}Sn_{33.3}$. The magnetic moment for $Mn_{50}Bi_{25}Sn_{25}$ is smaller than $(Mn_{0.5}Bi_{0.5})_{66.7}Sn_{33.3}$. However, the M_s in the unit of emu/g, emu/cm^3, and Tesla for $Mn_{50}Bi_{25}Sn_{25}$ is higher than that for $(Mn_{0.5}Bi_{0.5})_{66.7}Sn_{33.3}$. This is because the weight and volume of $Mn_{50}Bi_{25}Sn_{25}$ are smaller than $(Mn_{0.5}Bi_{0.5})_{66.7}Sn_{33.3}$.

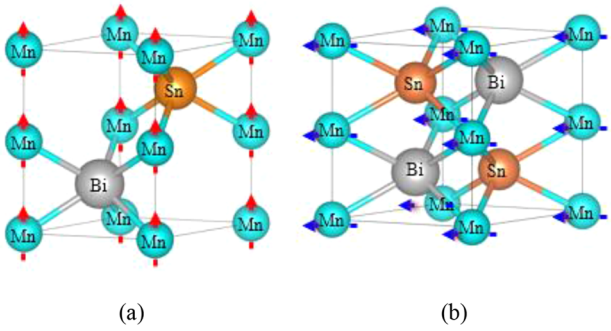

(a) (b)

FIG. 4. (a) Substitutionally Sn-doped MnBi with the out-of-plane spin direction and (b) interstitially Sn-doped MnBi with the in-plane spin direction.

The $(Mn_{0.5}Bi_{0.5})_{66.7}Sn_{33.3}$ has two more atoms in the unit cell, i.e., one more Bi and one more Sn than $Mn_{50}Bi_{25}Sn_{25}$.

To calculate the K_u, the magneto-crystalline anisotropy energy (MAE) of each MnBi system was calculated using the total energy difference between ⟨100⟩ and ⟨001⟩ spin configurations ($\Delta E = E_{\langle 100\rangle} - E_{\langle 001\rangle}$). One spin configuration is in the out-of-plane direction, and the other is in the in-plane. K_u was calculated to be −0.20 MJ/m^3 for MnBi, which agrees with measured K_u[6] and changes with the unit cell volume, as presented in Tables I and II Sn substitution for Bi in MnBi significantly increases K_u to 1.711 MJ/m^3 from

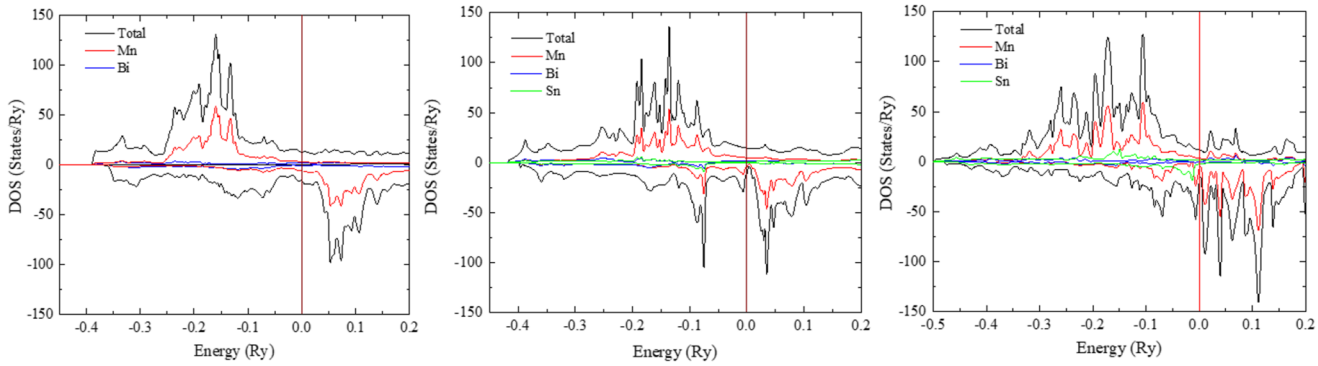

(a) (b) (c)

FIG. 3. Density of states for (a) LTP-MnBi, (b) $Mn_{50}Bi_{25}Sn_{25}$, and (c) $(Mn_{0.5}Bi_{0.5})_{66.7}Sn_{33.3}$.

TABLE II. Saturation magnetization (M_S) and magnetocrystalline anisotropy energy (MAE) and constant (K_u) for LTP-MnBi and Sn-doped MnBi.

Alloys	Magnetic moment (μ_B/f.u.)	Magnetic moment (emu/g)	M_S (emu/cm^3)	M_S (T)	MAE (meV/f.u.)	K_u (MJ/m^3)
$Mn_{50}Bi_{50}$	7.224	76.4	688	0.865	−0.122	−0.202
$Mn_{50}Bi_{25}Sn_{25}$	5.034	64.2	632	0.794	0.789	1.711
$(Mn_{0.5}Bi_{0.5})_{66.7}Sn_{33.3}$	6.609	48.2	585	0.736	−0.025	−0.043

TABLE III. Curie temperature for LTP-MnBi and substitutionally and interstitially Sn-doped MnBi.

Materials	No. of nearest neighbors			Distance (Å)			Exchange integral, J_0 (meV)	Curie temperature, T_C(K)
	z_{01}	z_{02}	z_{03}	r_{01}	r_{02}	r_{03}		
$Mn_{50}Bi_{50}$	2	6	2	3.056	4.287	6.118	69.523	716
$Mn_{50}Bi_{25}Sn_{25}$	2	6	2	2.728	3.954	5.456	57.557	445
$(Mn_{0.5}Bi_{0.5})_{66.7}Sn_{33.3}$	2	6	2	2.842	4.611	5.683	36.909	285

-0.202 MJ/m^3 of LTP-MnBi; therefore, the spin is in the out-of-plane, called spin reorientation, as shown in Fig. 4(a). On the other hand, when Sn is interstitially doped in MnBi, K_u remains negative, but slightly decreases to -0.043 MJ/m^3 from -0.202 MJ/m^3 of LTP-MnBi; therefore, the anisotropy remains in the in-plane as shown in Fig. 4(b). The calculated MAE and K_u are listed in Table II. Sn-doping decreases the valence electron 12 for MnBi to 5.79 for $Mn_{50}Bi_{25}Sn_{25}$. According to the band filling,[18] the MAE changes to the positive 1.711 MJ/cm^3 for $Mn_{50}Bi_{25}Sn_{25}$ from -0.2 MJ/m^3 of MnBi, leading to the out-of-plane magnetocrystalline anisotropy. This is the band filling effect on MAE.

For the temperature-dependent magnetization of the MnBi systems in this work, the supercell was constructed with two 1/3 hexagonal structures along the *a* axis or *c* axis to calculate Curie temperature (T_C) using Eq. (3). The significant exchange interactions over all the neighboring spins are, therefore, considered for the calculation of T_C. Table III summarizes the z_{ij} and r_{ij} and the calculated J_0 and T_C. The calculated J_0 decreases from 69.523 to 57.557 meV for the $Mn_{50}Bi_{25}Sn_{25}$ and 36.909 meV for the $(Mn_{0.5}Bi_{0.5})_{66.7}Sn_{33.3}$.

The calculated J_0 for LTP-MnBi agrees with the results in Ref. 6. However, the T_C estimated by Sakuma *et al.* is 560 K, much lower than the experimental T_C of 700 K.[5] On the other hand, our estimated T_C of 716 K is close to the experimental T_C, demonstrating that our computational method is reliable. Sn-doping in MnBi decreases T_C, and the interstitial Sn-doping degrades T_C more than the substitutional doping. The substitutional Sn-doping decreases T_C to 445 K from 716 K of MnBi, and the interstitial Sn-doping decreases T_C to 285 K. This is attributed to a decrease in exchange integral when Sn is doped. These estimated T_Cs are used to predict the temperature dependence of saturation magnetization in Fig. 5. Our predicted M_S(T) is in good agreement with the experimental data of Guo *et al.* (black dots in Fig. 5) for undoped MnBi, demonstrating our reliable computational method for M_S(T).

As the temperature increases, thermal energy (kT) increases against exchange energy (E_{ex}) and opposes spontaneously aligned magnetic dipoles, forming a spin cone, i.e., spin disorder. Thus, the width of the spin cone gets wider as the temperature increases until the temperature reaches the T_C, resulting in the disappearance of magnetic ordering. This leads to a decrease in the saturation magnetization.

Substitutional Sn doping changes the in-plane anisotropy to the out-of-plane, while the magnetocrystalline anisotropy direction remains unchanged when Sn is interstitially doping in MnBi. Magnetization at 300 K and Curie temperature of Sn-doped MnBi are too low to apply to synchronous permanent magnet motor; therefore, future work on lower Sn concentrated MnBi than the Sn concentration in this study.

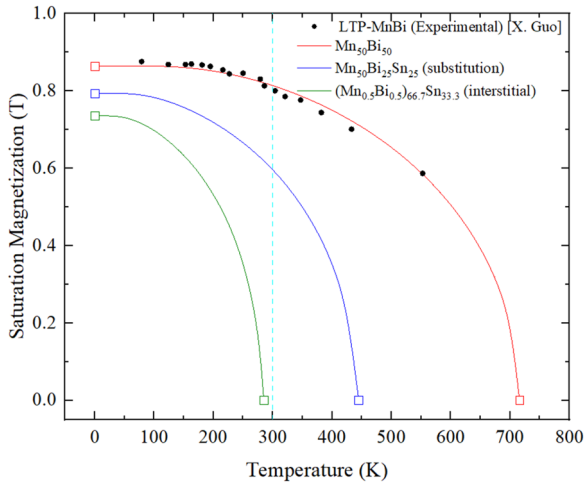

FIG. 5. Temperature dependence of M_s for LTP-MnBi and substitutionally and interstitially Sn-doped MnBi. The closed dot symbols represent experimental data, and the solid line is calculated from Eq. (4).

IV. CONCLUSION

Substitutional doping of Sn in LTP MnBi changes the magnetocrystalline anisotropy constant (K_u) from -0.202 MJ/m^3 (the in-plane magnetization) for LTP MnBi to 1.711 MJ/m^3 (the out-of-plane magnetization). In comparison, the K_u remains negative but slightly decreases to -0.043 MJ/m^3 when Sn is interstitially doped in MnBi.

Interstitial Sn-doping decreases Curie temperature (T_C) more rapidly than substitutional Sn-doping due to its smaller exchange integral (J_0). The magnetic moment (6.609 μ_B/f.u.) of interstitial Sn-doped MnBi is larger than the moment (5.034 μ_B/f.u.) of the substitutional Sn-doped MnBi.

ACKNOWLEDGMENTS

This work was supported in part by the National Science Foundation IUCRC under Grant No. 2137275 and the E. A. "Larry" Drummond Endowment at the University of Alabama.

AUTHOR DECLARATIONS

Conflict of Interest

The authors have no conflicts to disclose.

Author Contributions

Minyeong Choi: Conceptualization (equal); Data curation (equal); Formal analysis (equal); Investigation (equal); Methodology (equal); Software (equal); Validation (equal); Visualization (equal); Writing – original draft (equal); Writing – review & editing (equal). **Yang-Ki Hong**: Conceptualization (equal); Formal analysis (equal); Funding acquisition (equal); Investigation (equal); Methodology (equal); Project administration (equal); Supervision (equal); Writing – original draft (equal); Writing – review & editing (equal). **Hoyun Won**: Investigation (equal); Methodology (equal); Writing – original draft (equal); Writing – review & editing (equal). **Chang-Dong Yeo**: Conceptualization (equal); Formal analysis (equal); Investigation (equal); Methodology (equal); Project administration (equal); Supervision (equal); Writing – original draft (equal); Writing – review & editing (equal). **Byung-Chul Choi**: Formal analysis (equal); Investigation (equal); Methodology (equal); Writing – original draft (equal); Writing – review & editing (equal). **Jihoon Park**: Investigation (equal); Methodology (equal); Writing – original draft (equal); Writing – review & editing (equal). **Woncheol Lee**: Investigation (equal); Methodology (equal); Writing – original draft (equal); Writing – review & editing (equal).

DATA AVAILABILITY

The data that support the findings of this study are available from the corresponding author upon reasonable request.

REFERENCES

[1]T. Akiya, H. Kato, M. Sagawa, and K. Koyama, "Enhancement of coercivity in Al and Cu added Nd-Fe-B sintered magnets by high field annealing," IOP Conf. Ser.: Mater. Sci. Eng. **1**, 012034 (2009).
[2]J. Park, Y.-K. Hong, J. Lee, W. Lee, S.-G. Kim, and C.-J. Choi, "Electronic structure and maximum energy product of MnBi," Metals **4**, 455 (2014).
[3]See https://www.energy.gov/sites/prod/files/Session_A7_Hono_NIMS.pdf for the temperature coefficient of coercivity.
[4]X. Guo, X. Chen, Z. Altonunian, and J. O. Strom-Olsen, "Magnetic properties of MnBi prepared by rapid solidification," Phys. Rev. B **46**, 14578 (1992).
[5]B. W. Roberts, "Neutron diffraction study of the structures and magnetic properties of manganese bismuthide," Phys. Rev. **104**, 607 (1956).
[6]A. Sakuma, Y. Manabe, and Y. Kota, "First principles calculation of magnetocrystalline anisotropy energy of MnBi and $MnBi_{1-x}Sn_x$," J. Phys. Soc. Jpn. **82**, 073704 (2013).
[7]M. Choi, Y.-K. Hong, H. Won, G. J. Mankey, C. D. Yeo, W. Lee, M. H. Jung, T. Lee, and J. K. Lee, "Suppressing antiferromagnetic coupling in rare-earth free ferromagnetic MnBi-Cu permanent magnet," J. Appl. Phys. **129**, 113902 (2021).
[8]A. F. Andresen, W. Hälg, P. Fischer, E. Stoll, *et al.*, "The magnetic and crystallographic properties of MnBi studied by neutron diffraction," Acta Chem. Scand. **21**, 1543 (1967).
[9]Y. K. Hong, J. H. Park, O. N. Mryasov, S. G. Kim, S. Kim, J. Lee, G. S. Abo, C. J. Choi, and J. Lee, "Magnetic properties of MnBi based alloys: First-principles calculations for MnBi-Co and MnBi-Co-Fe cases," AIP Adv. **3**, 052137 (2013).
[10]P. Rania, A. Taya, and M. K. Kashyap, "Enhancement of magnetocrystalline anisotropy of MnBi with Co interstitial impurities," AIP Conf. Proc. **1942**, 130033 (2018).
[11]See https://www.iea.org/policies/15271-final-list-of-critical-minerals-2022 for the critical minerals.
[12]P. Blaha, K. Schwarz, G. K. H. Madsen, D. Kvasnicka, J. Luitz, R. Laskowsk, F. Tran, L. Marks, and L. Marks, *WIEN2K, An Augmented Plane Wave + Local Orbitals Program for Calculating Crystal Properties* (Karlheinz Schwarz, Techn Universitat, Wien, Austria, 2001).
[13]S. Ma, K. Bao, Q. Tao, P. Zhu, T. Ma, B. Liu, Y. Liu, and T. Cui, "Manganese mono-boride, an inexpensive room temperature ferromagnetic hard material," Sci. Rep. **7**, 43759 (2017).
[14]P. Novak and J. Rusz, "Exchange interactions in barium hexaferrite," Phys. Rev. B **71**, 184433 (2005).
[15]J. M. MacLaren, T. C. Schulthess, W. H. Butler, R. Sutton, and M. McHenry, "First principles study on the electronic structure and effective exchange interaction of $Y(Co_{1-x}Cu_x)_5$," J. Appl. Phys. **85**, 4833 (1999).
[16]B. D. Cullity and C. D. Graham, *Introduction to Magnetic Materials*, 2nd ed. (Wiley, Hoboken, NJ, 2009), p. 104.
[17]V. P. Antropov, V. N. Antonov, L. V. Bekenov, A. Kutepov, and G. Kotliar, "Magnetic anisotropic effects and electronic correlations in MnBi ferromagnet," Phys. Rev. B **90**, 054404 (2014).
[18]D. Wang, R. Wu, and A. J. Freeman, "First-principles theory of surface magnetocrystalline anisotropy and the diatomic-Pair model," Phys. Rev. B **47**, 14932 (1993).